PCCP

Accepted Manuscript

ROYAL SOCIETY OF CHEMISTRY

www.rsc.org/pccp

Electron transfers in a TiO_2-containing MOR zeolite: synthesis of the nanoassemblies and application using a probe chromophore molecule.

A. Legrand,[a] A. Moissette*[a], M. Hureau[a], S. Casale[b] , P. Massiani,*[,b,c] H. Vezin [a], A.S. Mamede[d], I. Batonneau-Gener[e]

[a] *LASIR, UMR 8516, Université Lille 1, Bât C8, 59655 Villeneuve d'Ascq cedex, France*
[b] *Sorbonne Universités, UPMC Université Paris 06, Laboratoire de Réactivité de Surface (LRS), 4 place Jussieu, 75005 Paris, France*
[c] *CNRS UMR 7197, UPMC, Laboratoire de Réactivité de Surface (LRS), 4 place Jussieu, 75005 Paris, France*
[d] *UCCS, CNRS UMR 8181, Ecole Nationale Supérieure de Chimie de Lille, Bât C3, 59655 Villeneuve d'Ascq cedex, France*
[e] *Institut de Chimie des Milieux et Matériaux de Poitiers (IC2MP), CNRS UMR 7285, Université de Poitiers, 4 rue Michel Brunet, 86022 Poitiers cedex*

Abstract - New assemblies constituted by a microporous matrix of mordenite (MOR) zeolite on which TiO_2 nanoclusters are deposited were synthesized using ionic oxalate complexes and $TiCl_3$ titanium precursors. The samples were used to investigate the transfers of electrons produced by spontaneous or photo-induced ionization of a guest molecule (t-Stilbene, t-St) occluded in the porous volume towards the conduction band of a conductive material placed nearby, in the pores or at least close to their entrance. The reaction mechanisms were compared in these Ti-rich solids and in a Ti-free mordenite sample. The characterizations by XRD, N_2 physisorption, TEM, XPS and DRIFT spectroscopy of the supramolecular TiO_2/MOR systems before t-St adsorption showed the preservation of the crystalline structure after Ti addition and thermal activation treatments. They also revealed that titanium is mainly located at the external surface of the zeolite grains, in the form of highly dispersed and/or aggregated anatase. After incorporation of the guest molecule in the new assemblies, diffuse reflectance UV-visible and EPR spectroscopies indicate that the electron transfer processes are similar with and without TiO_2 but strongly stabilized t-$St^{\bullet+}$ radicals are detected in the TiO_2-MOR samples whereas such species were never detected earlier in TiO_2-free mordenite using these techniques. The stabilization process is found more efficient in the sample prepared with $TiCl_3$ as precursor than with titanium oxalates. It is proposed that the proximity of TiO_2 with the formed t-$St^{\bullet+}$ radicals provokes the stabilization of the radical through capture of the ejected electron by the semi-conductor and that confinement effects can also play a role.

1. Introduction

In the last decades, many studies devoted to the synthesis of new complex molecular assemblies containing electron donor chromophores have been reported either in solution or in environments involving interfacial systems [1-7]. The strong interest for such systems comes from their ability to store charge separated states that can be stabilized at the molecular level and can be used to provide electron transfer capacity for applications in varying domains such as photovoltaic [3,8-17], energy [18-21], catalysis [22-31] or optics. [32-34] In that context, porous materials in which guest molecules can be incorporated are of high interest. By allowing a thorough control of the host-guest interactions, the large diversity and designability of these materials make them very useful in numerous applications. [35-38] Amongst the already tested solids, we recently demonstrated the ability of porous zeolites to stabilize such charge separated states for especially long periods after adsorption of aromatic molecules having dimensions similar to the pore size in the zeolite, which is commonly between 4 and 8 Å in diameter. [40-42] In addition to their organized microporous frameworks, an important advantage of zeolites is to offer a high surface area and a cationic exchange capacity that is expected to facilitate the ionization of the adsorbed aromatic molecules and to help creating persistent charge separated states. Moreover, even though the ionization process can be initiated either electrochemically [43] or by photoexcitation [42, 44-48] or radiolysis, [49-50] it can also occur spontaneously if the ionization potential of the molecule is sufficiently low and if the energy of polarization in the zeolite channel is high enough. [40] As a whole, stabilization of the separated charge states in the zeolite can thus be considered as an intrinsic property of the inner charged surface of the zeolite micropores space.

Besides the type of the adsorbed aromatic molecule, the effects of other parameters have been previously highlighted, related especially to the characteristics of the support itself that may strongly affect the ionization efficiency and the speed of recombination after charge separation. [51-54] These parameters are for instance the nature of the charge compensating cations (in particular protons), the opening of the pores mouth or the aluminium content. [55-56] In these previous studies, better understanding of the mechanisms involved in the ionization processes and of the key parameters leading to higher ionization efficiency has also been provided. However, even if the formation of charge separated states with good performances and life time is an important breakthrough, a crucial step for the system to be applicable lies on the possibility to capture the electrons after their initial ejection and trapping in the framework, which could be ensured by the use of microelectrodes coupled with the zeolitic

material. However, a specific problem is then encountered since zeolites are aluminosilicate materials, well known as insulators. As a consequence, it is necessary to find a way to exploit the very stable charge separated states present in the pores. Then, a promising solution could be to transfer the generated electrons towards the conduction band of a conductive material placed in the proximity of the stable charged chromophore, in the pores or at least close to their entrance.

Accordingly, the purpose of this study was to show the feasibility of such approach, by combining in a same material the zeolite support and a nanophase having semiconductive properties. To this end, semiconductor nanoclusters were synthesized at the surface and/or in the pores of the zeolite crystallites previous to the adsorption of the chromophore molecules, the final goal being to facilitate by this way the transfer of the electrons ejected during the ionization process to the conduction band of the semiconductor present nearby. More precisely, the purpose was to synthesize new assemblies constituted by a microporous matrix of mordenite (MOR) zeolite on which TiO_2 nanoclusters were deposited. The choice for this system was based on the well-known conducting properties of TiO_2 and on the mono-directional 12-membered ring pore system of the MOR structure in which the charge transfer was shown to be faster than in the smaller channels of FER or ZSM-5. [41,42] It can also be recalled that incorporation of TiO_2 in zeolites was previously reported in studies aimed at improving the photocatalytic efficiency of TiO_2, especially after visible light irradiation. [57-68] In these studies, titanium was added by either simple anchoring or by incorporation inside the zeolite cavities and mordenite was often selected as zeolite because of its hydrophobic properties and of its medium size mono-directional channels compatible with rod shape molecules. [47,69-72] The electron transfers in these systems were also shown to occur from the excited TiO_2 to the reactant molecule. In contrast, the electron transfer expected to take place in the present work should occur in the opposite way, from the guest molecule adsorbed within the zeolite voids towards the dispersed TiO_2 nanophase deposited on the support.

Three different titanium precursors will be used for samples preparation, namely two ionic oxalate complexes as already applied to exchange TiO^{2+} in the porosity of zeolites [58,69,73,74] and $TiCl_3$ that is more commonly found in studies dedicated to the synthesis of titanosilicates in which titanium is part of the framework, like in TS-1. [75] Nevertheless, $TiCl_3$ is known for its high solubility in water [76] and it has been used as precursor of TiO_2 nanoparticles in solution [77] or of TiO_2 nanospecies dispersed in zeolite Y. In the latter case, this compound

was used in its solid form that is highly reactive in the presence of air, which required working at low temperature (< 0°C) and under argon. [62]

After preparation, the supramolecular TiO_2/MOR systems will be characterized by various complementary techniques, namely XRD, N_2 physisorption, TEM, and DRIFT and DRUVv spectroscopies, with the aim to check the preservation of the structural and porous properties of the support and to identify the location and nature of the supported titanium phase. Next, diffuse reflectance UV-visible and EPR spectroscopies will be applied to investigate the electron transfer processes and analyse the effect, on the chromophore guest molecule, of the incorporation of the new assemblies. This will be made either directly or after previous (photo)excitation of the guest molecule that will be trans-Stilbene (t-St; (E)-1,2-diphenylethene), the first advantage of which being to present an appropriate molecular width (≈ 0.54 nm) to penetrate and diffuse into the MOR channels with 0.65 nm × 0.70 nm diameter aperture. [41,42,78] The second reason for choosing this chromophore is that its chemical and photochemical behaviours upon adsorption in various types of zeolite channels, especially MOR ones, were recently studied in the absence of TiO_2, [41,42] which will be of precious help for interpreting the present data.

2. Experimental

2.1. Materials

Preparation of the Ti-containing materials. The parent zeolite support was a commercial ammonium exchanged NH_4-MOR zeolite from Zeolyst International. Three Ti containing samples were prepared by adding titanium on the support, following the same exchange procedure in solution except for the nature of the titanium complex that was either an ammonium or potassium titanium oxalate complex ($M_2TiO(C_2O_4)_2$ with $M = NH_4^+$ or K^+, Sigma Aldrich) or titanium trichloride ($TiCl_3$, Alfa Aesar). The method consisted in dissolving the adequate titanium compound in water as to obtain a 0.2 M solution, afterwards 3g of the parent NH_4-MOR support was added. The suspension was stirred for 24 h at room temperature and this was performed under argon atmosphere to avoid TiO_2 formation that could occur, especially in presence of $TiCl_3$ (if contacted with air), and could lead to a loss of TiO_2 nanospecies in suspension. After recovery by filtration, the powders were washed with distilled water and dried overnight in an oven at 50°C. The procedure was repeated three times to increase the exchange levels. Finally, the parent zeolite and the three Ti containing

samples were calcined stepwise (50°C steps) till 450°C in static air, afterwards the atmosphere was switched to flowing Ar while keeping the temperature constant for 12h. The objective of this activation step was twofold: firstly, it allows converting the remaining NH_4^+ ions to gaseous ammonia (evolved in the gas phase) and to protons (which remain as exchangeable cations); secondly, it is expected to provoke the oxidation of the supported titanium phase needed to form the semi-conducting TiO_2 nanophase. Note that when using the $K_2TiO(C_2O_4)_2$ precursor, K^+ is expected to substitute the ammonium charge compensating cations. Accordingly, the four prepared samples will thereafter be denoted HMOR, TiO_2-$HMOR_{ox}$, TiO_2-$KMOR_{ox}$ and TiO_2-$HMOR_{Cl}$, where "ox" and "Cl" refer to the Ti precursor compound used for sample preparation.

Sorption of the organic guest molecule. Before sorption of the trans-stilbene (t-St) guest molecule, each calcined Ti-containing MOR sample was put in a closed quartz cell that was kept in dark and was heated up to 450°C in flowing dry Ar. Then, the sample was cooled to room temperature, a weighed amount of t-St corresponding to one t-St molecule per unit cell of zeolite (1 t-St / 48 T atoms) was introduced, and the cell was gently shaken in order to ensure good mixing between the zeolite and the t-St molecules. The powders were then transferred under dry argon either in a quartz glass Suprasil cell (for DRUVv experiments) or in cylindrical quartz tube (for EPR experiments) that were next sealed. Finally, the powder mixtures were left at room temperature (dry Ar and dark) to allow progressive sublimation of the trans-stilbene molecules and adsorption in the Ti-containing zeolite support until complete sorption. The generation of radicals was studied either directly (spontaneous ionization) or after photoexcitation of the sample at room temperature using excitation pulses at 300 nm (7 to 8 ns, 1.5 mJ) delivered by a 20 Hz Panther EX OPO tunable laser (Continuum, GSI group).

2.2. Physicochemical characterization techniques

The preservation of the zeolite structure along the treatments was verified by X-ray powder diffraction (XRD) using a Bruker D8 Advance series instrument, operating in the reflection mode with a Cu K_α radiation source generated at 40 kV and 40 mA. The diffraction scans were measured from 5 to 50° 2Θ with a 0.02° step and 2 s count time per step.

Nitrogen adsorption–desorption isotherms were performed at -196°C using the TRISTAR gas sorption system from Micromeritics in order to determine the textural properties. Before analysis, the samples were outgassed at 200 °C for 5 h under secondary vacuum (the parent material was degassed at 350°C).

The zeolite and Ti phase morphologies as well as the local chemical compositions were evaluated by Transmission Electronic Microscopy (TEM) on a high resolution LaB6 JEOL JEM 2011 instrument, operated with an acceleration voltage of 200 kV and equipped with an Energy Dispersive X-Ray spectrometer (EDXS). In order to ensure correct observation of the core of the grains, the micrographs were registered on thin 70 nm microtomic slices obtained on a Leica's microtome (after putting the sample in a resin).

2.3. Spectroscopic methods

Diffuse Reflectance Infrared Fourier Transform (DRIFT) spectra were registered on an infrared Nicolet Magna 860 apparatus equipped with a liquid-nitrogen-cooled MCT detector (Mid-IR), using the suitable beam splitter. The spectra, reported in Kubelka-Munk units, were the results of 1064 scans recorded with a 2 cm^{-1} resolution.

The surface compositions and nature of the species were analysed by X-ray Photoelectron Spectroscopy (XPS) using a Kratos Analytical AXIS Ultra^{DLD} spectrometer. A monochromatized aluminium source (Al K_α = 1486.6 eV) was used for excitation. The analyser was operated in constant pass energy of 40 eV using an analysis area of approximately 700 µm x 300 µm. Charge compensation was applied to overcome the charging effect occurring during the analysis. So the Si 2p (103.5 eV) binding energy (BE) of the support was used as internal reference. The spectrometer BE scale was initially calibrated against the Ag $3d_{5/2}$ (368.2 eV) level. Pressure was in the 10^{-10} Torr range during the experiments. Simulation of the experimental photopeaks and chemical quantifications were carried out using a CasaXPS software. The Si, Al and Ti contents were also evaluated by dispersive X-ray fluorescence analysis on a SPECTRO X-LabPro.Diffuse Reflectance UV-visible absorption (DRUVv) spectroscopy was carried out on a Cary 6000i spectrometer equipped with an external integrating sphere (DRA-1800) that allowed recording the data in the diffuse reflectance mode. The spectra were recorded between 200 and 900 nm and are presented in Kubelka-Munk units. The SIMPLISMA (SIMPLe-to-use Interactive Self-modeling Mixture Analysis) approach was used to perform the multivariate curve resolution data processing of the DRUVv spectral set $F(\lambda,t)$. [79] This method allowed extracting the individual spectral components and the respective concentration C(t) from the successive spectra registered as a function of time after the powder was mixed with the t-St host molecule. The kinetics were analyzed through the C(t) concentration decays that were accurately fitted using the Albery function which takes into account the heterogeneity of the material. [80]

The continuous wave (CW) Electronic Paramagnetic Resonance (EPR) spectroscopic experiments were carried out at room temperature with a Bruker X-band ELEXYS E580E spectrometer to investigate the fate of unpaired electrons after t-St ionization.

3. Results and discussion

3.1. Structural and textural properties

Characterization of the HMOR, TiO_2-$HMOR_{ox}$, TiO_2-$KMOR_{ox}$ and TiO_2-$HMOR_{Cl}$ samples was performed by complementary techniques before trans-stilbene adsorption to obtain information on the structural, porous and chemical properties of the prepared materials. A special attention was paid to the location and crystalline nature of the TiO_2 semiconductor nanoclusters expected to be present after Ti deposition and calcination.

Figure 1 compares the X ray diffractograms of the parent and Ti-enriched zeolites. For all samples, the peak positions and peak intensities remain the same, showing that the MOR crystalline structure was preserved after Ti addition in solution and activation at 450°C, whatever the titanium precursor. In addition, no diffraction peaks typical to either anatase (d_{101} peak expected around 25.3°) or rutile (d_{110} peak expected at 27.5°) [81] was detected, indicating that the supported Ti-based nanophases, if present, are either amorphous or in the form of clusters too small (below few nm) to be observable by XRD.

The preservation of the microcrystalline structure after Ti addition and thermal activation was also confirmed by nitrogen adsorption-desorption experiments at 77 K. The isotherms are of Type I (IUPAC classification) as exemplified in Figure 2 for the HMOR, TiO_2-$HMOR_{ox}$ and TiO_2-$HMOR_{Cl}$ zeolites. From the textural characteristics derived from these curves (Table 1), a significant increase of the microporous and mesoporous volumes is noted for sample TiO_2-$HMOR_{Cl}$ prepared with the $TiCl_3$ precursor, which may indicate that some framework dealumination and/or local dissolution took place during preparation. Indeed, it was previously reported for the MOR zeolite structure which structure contains side pockets that dealumination - which occurs preferentially at lattice defects - can lead to an increased microporosity by opening the entrance to the side pockets and connecting them to the adjacent channels, thus generating secondary micropores. [82] Besides, extraction of some extra framework species from the porosity during $TiCl_3$ treatment cannot be excluded.

Transmission Electron Microscopy was used to get information on the morphological and Ti location features that were comparable in all Ti-enriched samples. Micrographs of 50 nm

thick ultramicrotomic slices are shown in Figure 3, taking TiO_2-MOR_{Cl} as a representative sample. The low-magnification picture shows the general shape of the MOR grains, with sizes in the range 0.1-1 μm (Figure 3A), whereas the crystalline state of the zeolite grains and their microporous channel system clearly appear in the high-resolution (HR-TEM) mode (Figure 3B), thus attesting again of the zeolite network preservation after Ti deposition and thermal activation (Figure 3B). Nevertheless, black spots as well as aggregates are also observed on the surface of the zeolite crystallites, highly dispersed all over the sample (Figure 3C), that were shown to correspond almost exclusively to a titanium and oxygen rich phase as indicated by local chemical analyses carried out by energy-dispersive X-ray spectroscopy (EDX, data not detailed). On the contrary, the Ti content was always found limited (atomic Ti/Al ratio below 5 %) on zones of the MOR grains where such external nanospecies were absent. Interestingly, chlorine was also not detected, even on the TiO_2-MOR_{Cl} sample prepared with $TiCl_3$. Finally, HR-TEM observations show that the dispersed Ti-rich nanophases are composed of small spherical nanocrystals about 2 to 5 nm in diameter (Figure 3D) having lattice *d*-spacing values equal to 3.5 Å and 2.3 Å, as determined from their diffraction pattern (Figure 3E), which fits very well the values expected for the (101) and (103) crystallographic planes of anatase. [83] Therefore, it can be concluded from these data that titanium is mainly present in the form of highly dispersed and/or aggregated anatase located at the external surface of the zeolite crystallites, but in close contact with the grains. A minor part of titanium can be also incorporated in the zeolite channels but in lesser amount and in the form of TiO_2 nanoparticles too small to be detected by XRD measurements. [65]

3.2. Acidic properties and state of the supported Ti-based nanoclusters

Figure 4 shows the evolution upon calcination of the DRIFT spectra of the MOR samples previously exchanged in the $K_2TiO(C_2O_4)_2$ and $TiCl_3$ suspensions, then washed and dried at 50°C. For this study, the freshly prepared Ti-containing powders were placed in the reaction chamber of the Praying Mantis accessory before the temperature was raised from room temperature up to 450°C. For both samples, the spectra at room temperature (Figures 4a,a') show a band of lattice terminal silanol groups around 3738 cm^{-1} that did not evolve with temperature. For TiO_2-$HMOR_{Cl}$, a new band centred around 3605 cm^{-1} emerged when reaching 200°C (Figure 4c), which is typical of the ν(OH) modes of Brønsted acid Al-O(H)-Si sites, [78,84,85] thus attesting the conversion into protons of the NH_4^+ ions initially present in the samples. This band was still present after cooling, although slightly shifted (3595 cm^{-1}) as expected from the lattice deformation process occurring with temperature change (Figure 4f).

Interestingly, such Brønsted acid sites were absent in the case of TiO_2-$KMOR_{ox}$ that was prepared with the $K_2TiO(C_2O_4)_2$ precursor, revealing the good efficiency of the ammonium substitution by K^+ ions (Figure 4f'). Finally, the bands at 3655 and 3575 cm^{-1} visible at room temperature for both samples (either before heating or after heating and cooling) are due to hydration water.

Unfortunately, the DRIFT spectra could not provide further information on the Ti-based nano-species due to the overlapping of the Si-O and Al-O vibrational modes with the Ti-O ones. Similarly, FT-Raman spectroscopy could not be used because of the important fluorescence of the small zeolite microporous crystallites themselves. Nevertheless, more knowledge on the Ti phase could be gained by performing X-ray photoelectron spectroscopy that informed on the presence of titanium and on its comparative content in the different samples depending on their preparation.

As XPS allows the determination of the elemental composition of the sample surface (within the top 1-5 nm), this technique provided semi-quantitative analyses that were assumed to be representative in first approximation of the bulk of the sample. Table 2 reports the atomic concentrations (% at.) and photopeaks binding energy (BE) values of the detected elements. The Si, Al and Ti atomic contents evaluated from X-ray fluorescence, also indicated in the Table, show good agreement between the values measured by both techniques. It can be seen from these data that the atomic ratio Si/Al is close in all samples (from 12 to 10), and of the order of the theoretical value of 10 expected for the commercial parent zeolite. Note, however, the small increase of the Si/Al ratio - especially for sample TiO_2-$HMOR_{Cl}$ - that seems to support the hypothesis of a slight framework dealumination during preparation as already suggested by N_2 physisorption experiments. Secondly, data in Table 2 reveal that the Ti concentration is about three times higher in sample TiO_2-$HMOR_{Cl}$ than in TiO_2-$HMOR_{ox}$ and TiO_2-$KMOR_{ox}$ that were prepared with the cationic oxalate precursors. Thirdly, the presence of potassium in TiO_2-$KMOR_{Cl}$ is confirmed, with an atomic concentration (2.7 % at.) that is very close to that of aluminium (2.4 % at.), with no evidence of nitrogen, suggesting a full exchange of the NH_4^+ ions by K^+ ones during the preparation step in suspension, as already deduced from DRIFTS data. Fourthly, chlorine is never detected, in line with TEM observations.

In order to provide additional information on the Ti-based nanospecies, a deeper analysis of the XPS spectral features was carried out, in the binding energy ranges characteristic of the core electrons emitted by titanium and oxygen atoms. As example, Figure 5 shows the spectra

recorded in the case of the TiO_2-$HMOR_{Cl}$ sample. The photopeaks at 459.1 and 465.0 eV (Figure 5a) correspond to the Ti $2p_{3/2}$ and Ti $2p_{1/2}$ doublet lines, respectively. These BE values are similar to those reported for octahedrally coordinated titanium in TiO_2, [86] which confirms again that the exchanged and/or impregnated titanium species were transformed to TiO_2 upon thermal activation, in line with TEM observations. Interestingly, no signal was detected at lower BE value, around 457 eV, indicating the absence of Ti^{3+}. [87] With respect to oxygen, the two O_{1s} contributions observed at ~533 eV and ~531 eV can be attributed to oxygen atoms bound to tetrahedral framework (Si or Al) atoms and titanium atoms, respectively. [86,88] This attribution fits very well with the respective peak areas that represent 92% and 8% of the O_{1s} total signal. Indeed, with such attribution, the oxygen content in the Ti-based nanophase would represent 5.3 % of total atoms (i.e. of 66.9 x 0.08, Table 2) and the $O_{(531\ eV)}$/Ti atomic ratio is then equal to 2.2, in very good agreement with the expected value of 2 if considering that the whole content of titanium is under the TiO_2 form (1 Ti atom for 2 oxygen atoms).

Finally, UV-Visible spectra of the TiO_2-MOR samples were recorded before trans-stilbene adsorption, taking the HMOR zeolite as reference (spectra not shown). For all samples, a weak band was observed between 230 and 300 nm, assignable to TiO_2 even if the maximum of absorption was blue shifted with respect to TiO_2 anatase (~310 nm). [8,69,86,89,90] The corresponding band gap energies of the titania clusters estimated by using the Tauc method were always higher in the prepared MOR samples (3.6, 3.8 and 4 eV for TiO_2-MOR_{Cl}, TiO_2-$HMOR_{ox}$ and TiO_2-$KMOR_{ox}$, respectively) than in anatase (3.3 eV). These data are consistent with those reported in the literature for analogous systems. [8,69,86,89,90] Indeed, the blue shifts observed for the maximum of absorption and for the band gap absorption edge are often explained by quantum size effects interpreted in terms of charge carrier confinement that induce changes in the optical and electronic properties of TiO_2. Presently, this shift supports the previous TEM observation of a small size (few nm) of the anatase-like species deposited on the MOR support compared to the size of the crystals in the anatase reference (about 9 nm as determined with the Scherrer formula). These findings show the influence of the surface and internal volume of the support that helps stabilizing the TiO_2 particles in the form of small nanospecies. Therefore, even if part of the TiO_2 particles is located on the external surface of the zeolite grains as seen by TEM experiments, the size quantification effect deduced from UV-vis data suggest that extremely small TiO_2 species are also present in the internal mordenite volume, with sizes in the subnanometer range as imposed by the mordenite micropore dimension. [47,58,59,60,61,63,65,69,90]

3.3 Sorption of t-St and effect of Ti addition

When a calculated quantity of white solid t-St corresponding to 1 t-St per unit cell was contacted in the dark and under argon with dehydrated white TiO_2-$HMOR_{ox}$, TiO_2-$KMOR_{ox}$, TiO_2-$HMOR_{Cl}$, the powder remained white. The incorporation of t-St was monitored by conventional diffuse reflectance UV-visible absorption spectroscopy. The DRUVv spectra recorded one month after the mixing exhibit mainly an increase of the absorption band centered at 300 nm assigned to the neutral guest molecule. This evolution indicates the progressive sorption of t-St molecules in the porous space according to the adsorption mechanism described by equation 1:

$$\text{t-St} + TiO_2\text{-MOR} \rightarrow \text{t-St@}TiO_2\text{-MOR} \qquad \text{Eq. 1}$$

where t-St@TiO_2-MOR represents the molecule occluded in the TiO_2-MOR supports (presently TiO_2-$HMOR_{ox}$, TiO_2-$KMOR_{ox}$ or TiO_2-MOR_{Cl}).

In addition to the spectral features in the UV region, very weak broad bands in the 500-700 nm visible spectral range were observed after one month for TiO_2-$HMOR_{ox}$ and TiO_2-$HMOR_{Cl}$. These bands were the same as those previously observed after mixing the t-St with HMOR and assigned to the formation of a charge transfer complex occurring after the initial spontaneous ionization of the guest molecule (See Figure S1 A). [41] However, contrary to what was observed in the absence of TiO_2 (Figure S1 A), the intensity of these bands remained very weak in the case of TiO_2-$HMOR_{ox}$ and TiO_2-MOR_{Cl}, (see example in Figure 6a). Spontaneous ionization in high yield is usually considered to correlate with the presence of a highly polarizing environment such as H^+ acid sites. Then, the low ionization observed here might be due to a low accessibility to the acid sites or to a diffusion hindering due to the presence of the TiO_2 clusters at the pore entry or in the channels. Note also that spontaneous ionization was not detected after mixing t-St with the TiO_2-$KMOR_{ox}$; this observation is in line with the results of the sample characterization which suggest a full exchange of the NH_4^+ by K^+ ions as previous experiments showed that ionization only occurs after t-St photoexcitation in TiO_2 free KMOR (see figure S1 B). [42]

Due to the negligible spontaneous ionization in all prepared samples and in order to investigate properly the electron transfers in the supramolecular TiO_2-MOR systems, photoexcitation of the guest molecule was carried out previous to UV-Visible analyses. This was made three months after mixing the zeolites with the guest molecule to ensure that an equilibrium state was reached; note that the absorption band centered at 300 nm assigned to

the neutral t-St molecule did not evolve anymore after two months, and that the spectral features of the ionized species remaining moreover very weak. The irradiation of the white samples (1 cm × 1 cm area) was carried out using the 300 nm exciting line of a Panther EX OPO pulsed laser falling within the contour of the electronic transition of occluded t-St. A blue coloration was observed immediately after irradiation of the samples, and the evolution of the new photoinduced species was next immediately followed by DRUVv spectroscopy as a function of time, as illustrated for TiO_2-$HMOR_{Cl}$ (Figure 6).

Straight after the excitation of t-St@TiO_2-MOR_{Cl}, new characteristic absorption bands were observed in the visible domain at 476, 567, 626, and 694 nm in addition to the band centered at 300 nm assigned predominantly to occluded t-St (Figure 6b). The 476 nm band can be attributed to the t-$St^{\bullet+}$ radical cation by comparison with previous works on narrower pore zeolite like ferrierite and ZSM-5 [42] and on other media such as solid matrixes [91,92] or solution. [93,94] The broad band in the 500-700 nm region with 2 maxima at 567 and 626 nm is similar to the pattern already observed in acid mordenite after spontaneous ionization [41] and in non-acid mordenite after t-St photoexcitation. [42] This band is due to the hole transfer occurring after radical cation formation and is characteristic of the charge transfer complex (CTC, i.e. ***t-St@TiO***$_2$-$MOR^{\bullet+\bullet-}$) associated with an electron/hole pair. The guest molecule involvement in the electron/hole pair is demonstrated by the observation of a band structure that probably corresponds to vibronic transitions as the distances between the maxima are equal to 1662 cm^{-1} that is approximately the vibrational frequency of double CC bond. The mechanism of formation of this moiety depends on the oxidizing power of the radical and on the intrazeolite confinement as was already widely reported and discussed for this molecule and for other polyaromatics in channel type zeolites. [95] In the case of t-St in the TiO_2-MOR samples, the different steps involved in the photoreactivity mechanism can be written as follows:

t-St@TiO_2-MOR + hν → t-$St^{\bullet+}$@TiO_2-$MOR^{\bullet-}$ Eq. 2

t-$St^{\bullet+}$@TiO_2-$MOR^{\bullet-}$ $\xrightarrow{\bar{k}_{CTC}}$ t-St@TiO_2-$MOR^{\bullet+\bullet-}$ Eq. 3

t-$St^{\bullet+}$@TiO_2-$MOR^{\bullet-}$ $\xrightarrow{\bar{k}_{RC1}}$ t-St@TiO_2-MOR Eq. 4

t-St@TiO_2-$MOR^{\bullet+\bullet-}$ $\xrightarrow{\bar{k}_{RC2}}$ t-St@TiO_2-MOR Eq. 5

where ($\bar{k}_{RC1}$ + $\bar{k}_{CTC}$) represents the kinetic rate constant for the disappearance of the radical cation and $\bar{k}_{RC2,}$ the constant for CTC recombination.

The spectra recorded after irradiation clearly show a faster decrease of the 476 nm t-St$^{\bullet+}$ band intensity compared to the intensity of the 500-700 nm charge transfer complex bands (Figures 6c-f). Thus, the evolution of the CTC band indicates a slight increase of the CTC concentration at the expense of the t-St$^{\bullet+}$ in the first 15 minutes following the excitation (see comparison between Figures 6b and 6c). After 20 minutes, an intensity decay is observed for both transient species (t-St$^{\bullet+}$ and CTC) in favor of the band at 300 nm corresponding to the neutral t-St. The CTC bands are experimentally observed during 5 days whereas t-St$^{\bullet+}$ is no longer detected after 1 day (Figure 6e). The concentration decays C(t) which evolution are shown in Figure 7 were fitted using the Albery function which takes into account the heterogeneity of the material. [80] The lifetimes for t-St$^{\bullet+}$ and for the CTC are 65 minutes (k = $1/\tau$ = 0.0154 min^{-1}) and 260 minutes (k = 0.0038 min^{-1}), respectively. It is worth noting that the radical cation decay proceeds according to two parallel and competitive ways, and the associated rate constant determined by the Albery method has thus to take into account both the direct charge recombination and the hole transfer. Unfortunately, it is not possible to distinguish between both mechanisms. The direct recombination is, however, not preferred since the system leads mainly to the formation of the charge transfer complex. In the case of t-St occluded in TiO_2-$HMOR_{ox}$ and for TiO_2-$KMOR_{ox}$, analogous behaviors and identical transient species were obtained after photoexcitation, but with weaker band intensities and shorter lifetimes (table 3) that may be due to the lower titanium content in these samples.

In addition, to characterize the fate of the unpaired electrons after ionization and radical cation formation, the samples were analyzed using EPR technique. The CW EPR spectrum obtained at room temperature 5 minutes after irradiation of the t-St@TiO_2-MOR_{Cl} sample shows an hyperfine structure in the g=2 region characteristic of t-St$^{\bullet+}$ species (Figure 8). This feature is superimposed to a broad signal assigned to the ejected electron. This pattern evolved quickly to a narrower isotropic signal without any other contributions. The constant spectrum thus observed after one day is assigned to the electron/hole pair as already reported after t-St ionization in TiO_2-free mordenite as well as in ZSM-5 as in BEA zeolites. [96-98] Again, identical behaviors were observed for the three Ti-containing MOR samples but with weaker signal intensities and lower signal to noise ratios for t-St@TiO_2-$HMOR_{ox}$ and of t-St@TiO_2-$KMOR_{ox}$.

The longer lifetime of the radical cation observed in the TiO_2-containing MOR samples compared to the TiO_2-free zeolite demonstrates that the presence of TiO_2 in the material modifies the characteristics of the electron transfers occurring after t-St ionization. By allowing a transfer of the formed electron to the conduction band of the semi-conductor, the role of TiO_2 would then be analogous - although in a reverse way - to the one already thoroughly described in TiO_2 containing zeolite photocatalysts in which TiO_2 is added to provide electron mobility to the catalyst. For instance, it was reported that the incorporation of Ti dioxide within zeolite voids makes the photoactivity very different from that of bulk anatase, and it was shown that the activity depends on the zeolite type and on the TiO_2 loading, with significant photocatalytic rate enhancement for most investigated reactions. [47,58,62,63,64,69]. Interestingly, it was proposed that TiO_2 particles incorporated in the zeolite voids can act as electron relays favoring the electron transport from a photoexcited $Ru(bpy)_3^{2+}$ component located inside the zeolite to an external $Co(dphen)_3^{3+}$ acceptor. [64,99] In contrast, the photoelectron transfer between the $Ru(bpy)_3^{2+}$ electron donor and an electron acceptor molecule both encapsulated in zeolite Y cages was found less efficient when TiO_2 clusters containing only few Ti atoms were located between these species and the authors explained this feature by the much larger band gap for very small TiO_2 nanoclusters (1.3 nm) than for more classical TiO_2 particles (25-50 nm), the TiO_2 nanoclusters then hindering the interaction and acting more as insulators.[100] However, White and Dutta investigated more recently the coupling of CdS and TiO_2 semi-conductors in zeolite Y with the aim to prepare improved photocatalysts and they concluded that the electron transfer requires intimate contact between both encapsulated semi-conductors. [57]

With the help of above bibliography, various hypotheses can be considered to explain the role of TiO_2 in our materials. Firstly, the presence of TiO_2 nanoparticles mainly at the surface of the zeolite crystallites (as seen by TEM) could result in a partial blocking of the pore entries and in a hindering of the t-St diffusion into the pores that could contribute to the poor spontaneous ionization process due to t-St adsorption mainly on the external surfaces. However, this hypothesis has to be discarded because the ionization of t-St in such conditions would not lead to stabilization of long-lived transient species and especially would not allow hole transfer. Indeed, photoionization of t-St adsorbed only on the external surface of NaA zeolite because of 8-MR pores too narrow to accommodate t-St was found to induce solely t-$St^{\bullet+}$ formation and this radical could be detected only using time resolved spectroscopy due to its very short lifetime.[101] Consequently, the observation of highly stable charge separated

states with long life time is clearly in favor of t-St molecules occluded within the channels in the present TiO_2-MOR samples. Then, two possibilities can be envisaged: either the electrons migrate from the pores to the large TiO_2 clusters deposited on the external surface (as seen by TEM) or the electrons interact with the small subnanometer TiO_2 particles encapsulated in the channels (as deduced from DRUVv analyses).

At this point, the fate of the ejected electron in the zeolite and the process of electron-hole stabilization should be discussed. The existence of long life radical cations and CTC demonstrates that the unpaired electrons can be trapped in specific sites to delay recombination. Indeed, previous studies using pulsed EPR technique in similar but Ti-free systems showed the coupling between unpaired electrons and Al atoms of the framework as well as charge balancing cations suggesting electron trapping on the oxygen atoms close to Al atoms. Hence, the non-direct recombination and long lifetimes observed might be explained by electron hopping between various identical sites in the channels before final recombination. [102] Accordingly, such electron hopping from the initial ionization site to successive sites before reaching TiO_2 might be considered and thus migration of the electrons to TiO_2 located within the pores - or even on the external surface - might be envisaged. Then, both types of TiO_2 nanospecies inside and outside the pores could contribute to electron trapping in our samples and further work is being carried out to clarify the specific characteristics of the stabilization effect provided by each of them.

In conclusion, both DRUVv and EPR spectroscopies reveal the presence of long-life radical cation and very stable electron/hole pair species in the Ti containing samples, whereas in the absence of TiO_2, after mixing t-St with HMOR or after photoexcitation of t-St occluded in M-MOR (M = Na^+, K^+, Rb^+, Cs^+), the t-$St^{\bullet+}$ spectral features were never observed by conventional DRUVv (Figure S1) or EPR. In these Ti-free samples, the signal characteristic of t-$St^{\bullet+}$ was only observed using time resolved diffuse reflectance UV-vis spectroscopy on the nano-millisecond time scale. [42] Thus, even if the reaction mechanisms take place in similar way with and without TiO_2, the presence of the semi-conductor clearly slows down the electron-hole recombination in the porous volume indicating that a possible electron transfer to the conduction band of the semi-conductor has to be considered. In addition, it is important to remind that previous studies have clearly demonstrated the increase of the electron transfer kinetic when going from the narrow pore ferrierite to ZSM-5 and to MOR. [41,42] The high confinement effect in the zeolite channels is then a key parameter to stabilize t-$St^{\bullet+}$ for long times. Therefore, in the present case, it might be necessary to consider the increase of the

confinement effect due to the presence of TiO_2 in close proximity of the occluded molecule to explain the observation of t-$St^{\bullet+}$ in TiO_2/H-MOR whereas this moiety was never observable on this time scale in TiO_2-free H-MOR.

4. Conclusions

Through the various results obtained in this study, it appears that the inclusion of t-St in the channels of TiO_2-containing porous materials is a very promising approach for the stabilization for long periods of charge separated states created by photoexcitation. The diffusion properties as well as the distribution and the nature of the adsorption sites are actually essential factors to understand the photochemical reactions in zeolites. In particular, we highlight here the stabilization of t-$St^{\bullet+}$ in TiO_2-MOR whereas this species has so far never been detected by conventional UV-visible spectroscopy. Only experiments performed using time-resolved spectroscopy had demonstrated its formation. Thus, the proximity of TiO_2 with t-$St^{\bullet+}$ is put forward, to explain the stabilization of the radical through the capture of the ejected electron by the semi-conductor. It is also possible that the presence of TiO_2 in the pore volume of the zeolite, even in low amount, reduces the internal microporous volume and induces an effect of additional confinement affecting the electron transfer by slowing the recombination of the radical cation. Although more work would be needed to improve the method of incorporation of Ti not only on the surface but also in high yield at the interior of the mordenite porous network, it can be already concluded that using the $TiCl_3$ precursor was more efficient than the method carried out in presence of titanium oxalates. Finally, in the presence of TiO_2, almost no spontaneous ionization process took place making photoinduced ionization necessary.

References

(1) L. Kobr, D.M. Gardner, A.L. Smeigh, S.M. Dyar, S.D.; Karlen, R. Carmieli, M.R. Wasielewski, *J. Am. Chem. Soc.* **2012**, *134*, 12430-12433.

(2) A.B. Ricks, K.E. Brown, M. Wenninger, S.D. Karlen, Y.A. Berlin, D.T. Co, M.R. Wasielewski, *J. Am. Chem. Soc.* **2012**, *134*, 4581-4588.

(3) J. Hankache, M. Niemi, H. Lemmetyinen, O. S. Wenger, Hydrogen-Bonding Effects on the Formation and Lifetimes of Charge-Separated States in Molecular Triads. *J. Phys. Chem. A* **2012**, *116*, 8159-8168.

(4) P. K. Dutta, M. Severance, *J. Phys. Chem. Lett.* **2011**, *2*, 467-476.

(5) G. Calzaferri, R. Meallet-Renault, D. Bruhwiler, R. Pansu, I. Dolamic, T. Dienel, P. Adler, H-R Li, A. Kunzmann, *ChemPhysChem* **2011**, *12*, 580-594.

(6) G. Calzaferri, H. Li, D. Bruhwiler, *Chem-Eur. J.* **2008**, *14*, 7442-7449.

(7) P. G. Hoertz, T. E. Mallouk, *Inorg. Chem.* **2005**, *44*, 6828-6840.

(8) M. Alvaro, E. Carbonell, P. Atienzar, H. Garcia, *ChemPhysChem* **2006**, *7*, 1996-2002.

(9) J. R. Durrant, S. A. Haque, E. Palomares, *Chem. Commun.* **2006**, 3279-3289.

(10) G. Calzaferri, S. Huber, H. Maas, C. Minkowski, *Angew. Chem., Inter. Ed.* **2003**, *42*, 3732-3758.

(11) P. Atienzar, S. Valencia, A. Corma, H. Garcia, *ChemPhysChem* **2007**, *8*, 1115-1119.

(12) A. De la Escosura, M.V. Martinez-Diaz, D.M. Guldi, T. Torres, *J. Am. Chem. Soc.* **2006**, *128*, 4112-4118.

(13) M. E. El-Khouly, A. M. Gutierrez, A. Sastre-Santos, F. Fernandez-Lazaro, S. Fukuzumi, *Phys. Chem. Chem. Phys.* **2012**, *14*, 3612-3621

(14) P. V. Kamat, *J. Phys. Chem. C* **2008**, *112*, 18737-18753.

(15) A. J. Cowan, J. R. Durrant, *Chem. Soc. Rev.* **2013**, *42*, 2281-2293.

(16) A. Listorti, B. O'Regan, J. R. Durrant, *Chem. Mat.* **2011**, *23*, 3381-3399.

(17) A. A. Bakulin, S. D. Dimitrov, A. Rao, P. C. Y. Chow, C. B. Nielsen, B.C. Schroeder, I. McCulloch, H. J. Bakker, J. R. Durrant, R. H. Friend, *J. Phys. Chem. Lett.* **2013**, *4*, 209-215.

(18) I. McConnell, G. Li, G. W. Brudvig, *Chem. Biol.* **2010**, *17*, 434-447.

(19) S. Hammes-Schiffer, *Accounts Chem. Res.* **2009**, *42*, 1881-1889.

(20) K. Ikeda, K. Takahashi, T. Masuda, K. Uosaki, *Angew. Chem., Inter. Ed.* **2011**, *50*, 1280-1284.

(21) C. C. Moser, P. L. Dutton, *Advances in Photosynthesis and Respiration*. **2006**, *24*(Photosystem I), 583-594.

(22) S. Sato, H. Nakamura, *Angew. Chem. Inter. Ed.* **2013**, *52*, 8681-8684.

(23) X. Yang, H. Wang, J. Li, W. Zheng, R. Xiang, Z. Tang, H. Yu, F. Peng, *Chem. Eur. J.* **2013**, *19*, 9818-9824.

(24) A. Fattori, L. M. Peter, H. Wang, H. Miura, F. Marken, *J. Phys. Chem. C* **2010**, *114*, 11822-11828.

(25) S. Fukuzumi, *Pure Appl. Chem.* **2007**, *796*, 981-991.

(26) G. Yang, L. Zhou, X. Liu, X. Han, X. Bao, *Chem. Eur. J.* **2011**, *17*, 1614-1621.

(27) N. V. Beznis, B. M. Weckhuysen, J. H. Bitter, *Catal. Lett.* **2010**, *138*, 14-22.

(28) L. Li, X.-S. Zhou, G.-D. Li, X.-L. Pan, J.-S. Chen, *Angew. Chem. Inter. Ed.* **2009**, *48*, 6678-6682.

(29) L. Pinard, S. Hamieh, C. Canaff, F. Ferreira Madeira, I. Batonneau-Gener, S. Maury, O. Delpoux, K. Ben Tayeb, Y. Pouilloux, H. Vezin, *J. Catal.* **2013**, *299*, 284-297.

(30) F. Ferreira Madeira, H. Vezin, N. S. Gnep, P. Magnoux, S. Maury, N. Cadran, *ACS Catal.* **2011**, *1*, 417-424.

(31) G. B. McVicker, G. M. Kramer, J. J. Ziemiak, *J. Catal.* **1983**, *83*, 286-300.

(32) K. R. J. Thomas, N. Kapoor, C.-P. Lee, K.-C. Ho, *Chem. Asian J.* **2012**, *7*, 738-750.

(33) C.T. Hsiao, S.Y. Lu, *J. Mater. Chem.* **2009**, *19*, 6766-6772.

(34) S. R. Gonzalez, J. Orduna, R. Alicante, B. Villacampa, K. A. McGee, J. Pina, J. Seixas de Melo, K. M. Schwaderer, J.C. Johnson, B. A. Blackorbay, et al. *J. Phys. Chem. B* **2011**, *115*, 10573-10585.

(35) M. E. Medina, A. E. Platero-Prats, N. Snejko, A. Rojas, A. Monge,; F. Gandara,; E. Gutierrez-Puebla, M. A. Camblor, *Advanced Materials* **2011,** *23*, 5283-5292.

(36) T. D. Bennett, A. K. Cheetham, *Acc. Chem.Res.* **2014**, dx.doi.org/10.1021/ar5000314

(37) J. Jiang, R. Babarao,; Z. Hu, *Chemical Society Reviews* **2011**, *40*, 3599-3612. |

(38) T. Yamada, K. Otsubo, R. Makiura, H. Kitagawa, *Chem. Soc. Rev*. **2013**, *42*, 6655-6669.

(39) K. Ariga, A. Vinu, Y. Yamauchi, Q. Ji, J. P. Hill, *Bull. Chem. Soc. Jpn.* **2012**, *85*, 1-32.

(40) S. Carre, F. Luchez, A. Moissette, O. Poizat, I. Batonneau-Gener, *ChemPhysChem* **2012**, *13*, 504-513.

(41) M. Hureau, A. Moissette, H. Vezin, C. Bremard, M. Orio, *J. Phys. Chem. C* **2012**, *116*, 1812-1825.

(42) M. Hureau, A. Moissette, A. Legrand, F. Luchez, M. Sliwa, C. Bremard, *J. Phys. Chem. C* **2012**, *116*, 9092-9105.

(43) D. R. Rolison, *Chem. Rev.* **1990**, *90*, 867-878.

(44) X. Liu, Y. Mao, S. A. Ruetten, J. K. Thomas, *Sol. Energ. Mat. Sol. C.* **1995**, *38*, 199-219.

(45) S. Sankararaman, K. B. Yoon, T. Yabe, J. K. Kochi, *J. Am. Chem. Soc.* **1991**, *113,* 1419-1421.

(46) R. Jono, K. Yamashita, *J. Phys. Chem. C* **2012**, 116, 1445-1449.

(47) Y.I. Kim, S.W. Keller, J.S. Krueger, E.H. Yonemoto, G.B. Saupe, T.E. Mallouk, *J. Phys. Chem. B* **1997**, *101*, 2491-2500.

(48) E. H. Yonemoto, Y. I. Kim, R. H. Schmehl, J. O. Wallin, B. A. Shoulders, B. R. Richardson, J. F. Haw, T. E. Mallouk, *J. Am. Chem. Soc.* **1994**, *116*, 10557–10563.

(49) J. K. Thomas, *Chem. Rev.* **2005**, *105*, 1683-1734.

(50) X.Z. Qin, A. D. Trifunac, *J Phys. Chem* **1990**, *94,* 4751-4754.

(51) F. Belhadj, A. Moissette, C. Bremard, M. Hureau, Z. Derriche, *ChemPhysChem* **2011**, *12*, 1378-1388.

(52) J. C. Scaiano, H. Garcia, *Acc. Chem. Res.* **1999**, *32*, 783-793.

(53) A. E. Keirstead, N. P. Schepp, F. L. Cozens, *J. Phys. Chem. C* **2007**, *111*, 14247-14252.

(54) S. Hashimoto, *J. Photochem. Photobiol. C* **2003**, *4*, 19-49.

(55) A. Moissette, F. Belhadj, C. Brémard, H. Vezin, *Phys. Chem. Chem. Phys.* **2009**, *11*, 11022-11032.

(56) I. Gener, A. Moissette, C. Brémard, *Phys. Chem. Chem. Phys.* **2004**, *6*, 3732-3738.

(57) J.C. White, P.K. Dutta, *J. Phys. Chem. C* **2011**, *115*, 2938-2947.

(58) S. Anandan, M. Yoon, *J. Photochem. Photobiol. C* **2003**, *4*, 5-18.

(59) M. Takeuchi, M. Hikada, M. Anpo, *J. Hazard. Mat.* **2012**, *237-238*, 133-139.

(60) B. Cojoracu, S. Neatu, V.I. Parvulescu, K. Dumbuya, H.-P. Steinruck, J.M. Gottfried, C. Aprile, H. Garcia, J.C. Scaiano *Phys.Chem.Chem.Phys.* **2009**, *11*, 5569-5577.

(61) C. Aprile, A. Corma, H.Garcia, *Phys.Chem.Chem.Phys.* **2008**, *10*, 769–783.

(62) S.H. Bossmann, S. Jockush, P. Schwarz, B. Baumeister, S. Göb, C. Schnabel, L. Payawan Jr., M.R. Pokhrel, M. Wörner, A.M. Braun, N. Turro, *J. Photochem. Photobiol. Sci.* **2003**, *2*, 477-486.

(63) G. Cosa, M.S. Gallero, L. Fernandez, F. Marquez, H. Garcia, J.C. Scaiano, *New J. Chem.* **2002**, *26*, 1448-1455.

(64) S.H. Bossmann, C. Turro, C. Schnabel, M.R. Pokhrel, L.M. Payawan Jr., B. Baumeister, M. Wörner, *J. Phys. Chem B* **2001**, *105*, 5374-5382.

(65) M. Takeuchi, T. Kimura, M. Hikada, D. Rakhmawaty, M.Anpo, *J. Catal.* **2007**, *246*, 235-240.

(66) D.I. Petkowicz, R. Brambilla, C. Radtke, C.D. Silva da Silva, Z.N. da Rocha, S.B.C. Pergher, J.H.Z. dos Santos, *Appl. Catal. A* **2009**, *357*, 125-134.

(67) J. Sun, S. Zhai, Z. Xiao, Q. An, D. Huang, *Materials Science in Semiconductor Processing*, **2014**, http://dx.doi.org/10.1016/j.mssp.2014.01.003

(68) J. Klaas, G. Schulz-Ekloff, N. I. Jaeger, *J. Phys. Chem. B* **1997**, *101*, 1305.

(69) X. Liu, K. K. Iu, J. K. Thomas, *J. Chem. Soc. Faraday Trans.* **1993**, *89*, 1861-1865.

(70) M. Kitano, M. Matsuoka, M. Ueshima, M. Anpo, *Appl. Catal. A* **2007**, 325, 1-14.

(71) M. Takeuchi, S. Sakai, A. Ebrahimi, M. Matsuoka M. Anpo, *Top. Catal.* **2009**, *52*, 1651-1659.

(72) M. Takeuchi, J. Deguchi, M. Hikada, S. Sakai, K. Woo, P.-P. Choi, J.-K. Park, M. Anpo, *Appl. Catal. B* **2009**, 89, 406-410.

(73) J. Zhang, Y. Hu, M. Matsuoka, M. Yamashita, M. Minagawa, H. Hidaka, M. Anpo, *J. Phys. Chem. B* **2001**, *105*, 8395-8398.

(74) G. Zhang, W. Choi, S.H. Kim, S.B. Hong, *J. Hazard. Mater.* **2011**, *188*, 198-205.

(75) X. Wang, P. Zhang, X. Liu, B. Zhang, *Appl. Surf. Sci.* **2007**, *254*, 544-547.

(76) M. Kakihana, M. Kobayashi, K. Tomita, V. Petrykin, *Bull. Che. Soc. Japan*, **2010**, *83*, 1285-1308.

(77) E. Acayanka, A. Tiya Djowe S. Laminsi, C. C. Tchoumkwe, S. Nzali, A. Poupi Mbouopda, P. T. Ndifon, E. M. Gaigneaux, *Plasma Chem. Plasma Process.* **2013,** *33*, 725–735

(78) O. Marie, P. Massiani, F. Thibault-Starzyk, *J. Phys. Chem. B* **2004**, *108*, 5073-5081.

(79) W. Windig, B. Antalek, J. L. Lippert, Y. Batonneau, C. Bremard, *Anal. Chem.* **2002**, *74*, 1371-1379.

(80) W.J. Albery, P.N. Bartlett, C.P. Wilde, J.R. Darwent, *J. Am. Chem. Soc.* **1985**, *107*, 1854-1858.

(81) K. Porkodi, S. D. Arokiamary, *Mater. Charact.* **2007**, *58,* 495–503.

(82) F. Goovaerts, E.F. Vansant, J. Phillipaerts, P. De Hulsters, J. Gelan, *J. Chem. Soc. Faraday Trans. I,* **1989**, *85*, 3675-3685.

(83) A. Roguska, M. Pisarek, M. Andrzejczuk, M. Dolata, M. Lewandowska, M. Janik-Czachor, *Mater. Sci. Engineer. C* **2011**, *31*, 906–914.

(84) A. Bhan, A.D. Allian, G.J. Sunley, D. J. Law, E. Iglesia, *J. Am. Chem. Soc*., **2007**, *129*, 4919-4924.

(85) M. Maache, A. Janin, J.C. Lavalley, E. Benazzi, *Zeolites*, **1995**, *15*, 507-516.

(86) G. Lassaletta, A. Fernandez, J. P. Espinos, A. R. Gonzalez-Elipe, *J. Phys. Chem.* **1995**, *99*, 1484–1490.

(87) X. Noirfalise, F. Renaux, D. Cossement, N. Sebaihi, Lazzaroni, R. Snyders *Surf. Sci.* **2012**, *606* 1680–1684.

(88) B. M. Reddy, B. Chowdhury, I. Ganesh, E. P. Reddy, T. C. Rojas, A. Fernandez, *J. Phys. Chem. B* **1998**, *102*, 10176-10182.

(89) G. Li, L. Li, J. Boerio-Goates, B. F. Woodfield, *J. Am. Chem. Soc.* **2005**, *127*, 8659–8666.

(90) N. Satoh, T. Nakashima, K. Kamikura, K. Yamamoto, *Nat. Nanotechnol.* **2008**, *3*,106-111.

(91) Y. Kuriyama, S. Oishi, *Chem. Lett.* **1995**, *2*, 149-150.

(92) I. K. Lednev, N. Mathivanan, L. J. Johnston, *J. Phys. Chem.* **1994**, *98*, 11444-51.

(93) H. Ueda, *B. Chem. Soc. Jpn.* **1970**, *43*, 297-300.

(94) H. Miki, K. Yoshida, C. Kawate, R. Shimada, T. Takaya, K. Iwata, H. Hamaguchi, *Chem. Phys. Lett.* **2012**, *527*, 27-30.

(95) A. Moissette, M. Hureau, S. Carré, H. Vezin, P. Col *J. Phys. Chem. C* **2013**, *117*, 20625–20635.

(96) A. Moissette, C. Bremard, M. Hureau, H. Vezin, *J. Phys. Chem. C* **2007**, *111*, 2310-2317.

(97) A. Moissette, R. F. Lobo, H. Vezin, K. A. Al-Majnouni, C. Bremard, *J. Phys. Chem. C* **2010**, *114*, 10280-10290.

(98) R.F. Lobo, A. Moissette, M. Hureau, S. Carré, H. Vezin, A. Legrand, *J. Phys. Chem. C* **2012**, *116*, 14480−14490.

(99) G. Cosa, M. N. Chretien, M. S. Galletero, V. Fornes, H. Garcia and J. C. Scaiano, J. Phys. Chem. B, 2002, 106, 2460.

(100) M. Alvaro, M. N. Chretien, V. Fornes, M. S. Galletero, H. Garcia and J. C. Scaiano, J. Phys. Chem. B, 2004, 108, 16621.)

(101) K.-K. Iu, X. Liu, J. K. Thomas, *J. Photochem. Photobiol. A: Chemistry* **1994**, *79*, 103-107.

(102) M. Hureau, A. Moissette, J. Gaillard, C. Brémard, *Photochem. Photobiol. Sci.* **2012**, 11, 1515-1519.

Table 1: Textural characteristics deduced form nitrogen physisorption isotherms.

Sample	A_{BET} ($m^2.g^{-1}$)	V_{total}[a] ($cm^3.g^{-1}$)	V_{micro}[b] ($cm^3.g^{-1}$)	V_{meso}[c] $cm^3.g^{-1}$)
HMOR	540	0.28	0.20	0.08
TiO_2-$HMOR_{Cl}$	786	0.45	0.28	0.17
TiO_2-$HMOR_{ox}$	547	0.29	0.20	0.09

[a] Determined from nitrogen volume adsorbed at $P/P_0 = 0.995$
[b] Determined from t-plot analysis
[c] Determined from the difference between V_{total} and V_{micro}
A_{BET} : surface area measured by Brunauer, Emmet, Teller (BET) method.

V_{micro} = microporous volume; V_{meso} = mesoporous volume; $V_{total} = V_{micro} + V_{meso}$

Table 2: List of observed elements and related binding energies and atomic concentrations deduced from XPS data for the TiO_2-$HMOR_{Cl}$, TiO_2-$HMOR_{ox}$ and TiO_2-$KMOR_{ox}$ samples.

	HMOR	TiO_2-$HMOR_{Cl}$			TiO_2-$HMOR_{ox}$			TiO_2-$KMOR_{ox}$	
	Fluo X	XPS		Fluo X	XPS		Fluo X	XPS	
Element	(% at.)	BE (eV)	(% at.)	(% at.)	BE (eV)	(% at.)	(% at.)	BE (eV)	(% at.)
O 1s	n.d.	533.0 (92%) 531.0 (8%)	66.9	n.d.	532.8	68.7	n.d.	533.1	69.4
N 1s	n.d.	403.3	1.7	n.d.	403.0	1.4	n.d.		
Si 2p	22.6	103.5	26.8	24.7	103.5	26.9	24.3	103.5	24.6
Al 2p	2.0	74.8	2.2	2.0	74.8	2.2	2.1	74.7	2.4
Ti 2p	0.15	459.0	2.4	1.8	459.7	0.7	0.6	458.7	0.9
K								294.7	2.7
Si/Al*	11.3		12.2	12.3		12.2	11.6		10.3
Ti/Al	0.07		1.1	0.9		0.3	0.3		0.4

* the atomic Si/Al ratio for parent NH_4-MOR mordenite is 10 (commercial value given by Zeolyst)

Table 3: Kinetic Results of t-St$^{\bullet+}$@TiO_2/MOR $^{\bullet-}$ Decays and t-St@TiO_2/MOR$^{\bullet+\bullet-}$ Decays following 300 nm Photolysis of t-St@TiO_2/MOR

Zeolite	t-St$^{\bullet+}$@TiO_2/MOR$^{\bullet-}$		t-St@TiO_2/MOR$^{\bullet+}$ $^{\bullet-}$	
	τ (min)	k (min^{-1})	τ (min)	k (min^{-1})
HMOR [a]	Not observed		Spontaneous ionization	
KMOR [b]	0.0068*	147.06	24	0.0425
TiO_2/$HMOR_{ox}$	20	0.0512	70	0.01416
TiO_2/$KMOR_{ox}$	43	0.0234	109	0.00919
TiO_2/MOR_{Cl}	65	0.0154	259	0.00386

[a]: see ref. [41]

[b]: see ref. [42]

* observed using time resolved diffuse reflectance UV-vis spectroscopy

τ : lifetime and k : rate constant with k=1/τ

Figures captions

Figure 1: X-ray diffractograms of the MOR zeolites and of the TiO_2 anatase phase. The diffractogram of anatase is multiplied by 3 (y scale) for the sake of better clarity.

Figure 2: Nitrogen adsorption-desorption isotherms at 77 K on HMOR, TiO_2-$HMOR_{Cl}$ and TiO_2-$HMOR_{ox}$. P is the pressure at the equilibrium and P_0 is the saturated vapor pressure.

Figure 3: (A) representative transmission electron micrographs of a microtomic slice of TiO_2-$HMOR_{Cl}$ and (B) HR-TEM picture showing the preservation of the microporous channel structure in the zeolite grains; (C) enlargement on a zone showing the deposited Ti nanospecies, (D) HR-TEM image of these species and (E) related diffraction pattern revealing the d_{101} (3.5 Å) and d_{103} (2.3Å) plans typical of anatase. The HR-TEM images presented in (B) and (D) correspond to the areas circled in (A) and in (C), respectively. The diffraction pattern presented in (E) correspond to the smaller area circled on graph (C).

Figure 4 : DRIFT spectra during calcination of the MOR samples contacted with the (a-f) $TiCl_3$ and (a'-f') $K_2TiO(C_2O_4)_2$ solutions, then wahsed and dried (50°C): spectra registered at (a,a') 25°C, (b) 100°C or (b') 150°C, (c) 200°C, (d,d') 300°C, (e,e') 450°C and (f,f') 25°C after cooling. The spectra are vertically shifted for the sake of better clarity.

Figure 5: XPS spectra of TiO_2-$HMOR_{Cl}$ in the binding energies ranges characteristic of (a) Ti 2p and (b) O 1s.

Figure 6: DRUVv spectra recorded as a function of time after laser irradiation at 300 nm of t-St@TiO_2-$HMOR_{Cl}$ (a) before irradiation, (b) 5 min, (c) 15 min, (d) 5 h, (e) 10 h, (f) 24 h, (g) 1.5 day and (h) 3 days after photoexcitation.

Figure 7. Normalized decay profiles of C_t/C_0 relative to spectral concentration of (a) t-$St^{\bullet+}$@TiO_2-H-$MOR_{Cl}^{\bullet-}$ and (b) t-St@TiO_2-$HMOR_{Cl}^{\bullet+\bullet-}$ monitored at 476 nm and at 567 nm respectively after the 300 nm laser excitation. The solid line represents the best fit calculated decays using the Albery function; the squares represent the experimental points.

Figure 8. CW EPR spectra at room temperature after laser photoirradiation at 300 nm of t-St@TiO_2/$HMOR_{Cl}$; spectra recorded after (a) 10 min, (b) 2 h and (c) 1 day.

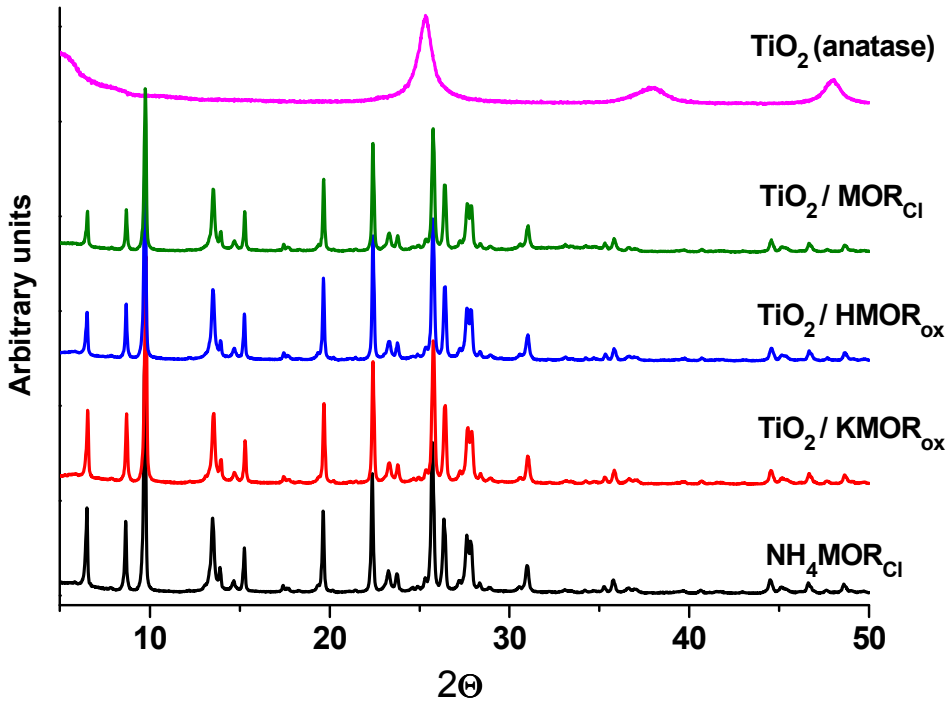

Figure 1: X-ray diffractograms of the MOR zeolites and of TiO_2 (anatase phase). The diffractogram of anatase is multiplied by 3 (y scale) for the sake of better clarity.

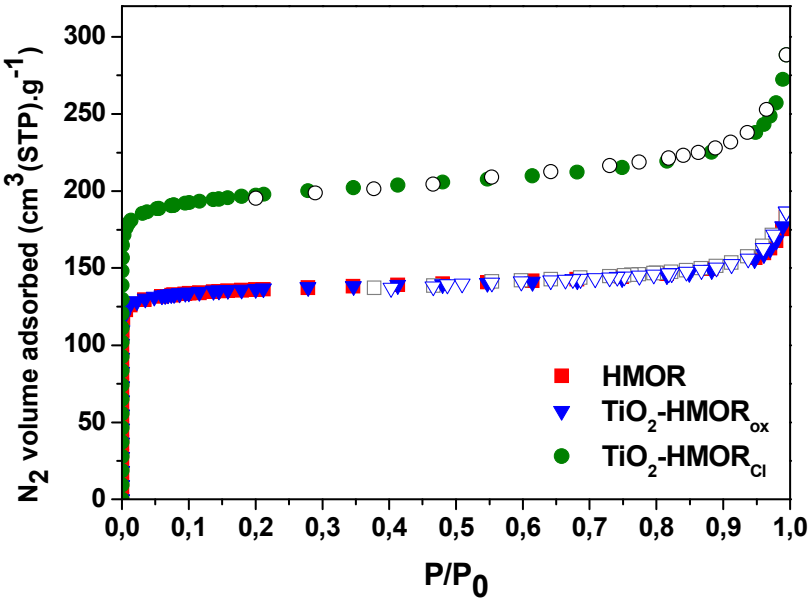

Figure 2: Nitrogen adsorption-desorption isotherms at 77 K on HMOR, TiO_2-$HMOR_{Cl}$ and TiO_2-$HMOR_{ox}$. P is the pressure at the equilibrium and P_0 is the saturated vapor pressure.

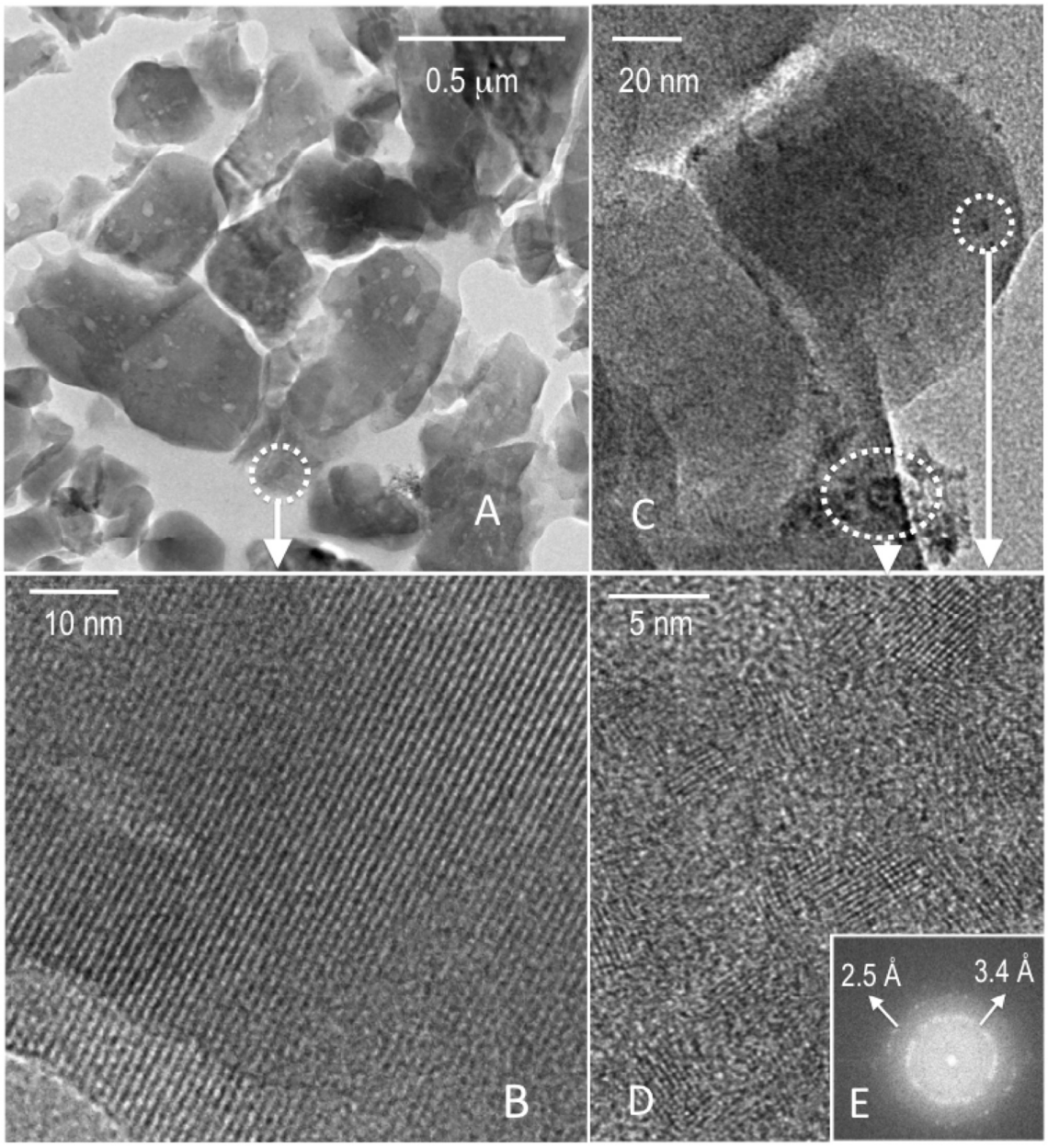

Figure 3: (A) representative transmission electron micrographs of a microtomic slice of TiO_2-$HMOR_{Cl}$ and (B) HR-TEM picture showing the preservation of the microporous channel structure in the zeolite grains; (C) enlargement on a zone showing the deposited Ti nanospecies, (D) HR-TEM image of these species and (E) related diffraction pattern revealing the d_{101} (3.5 Å) and d_{103} (2.3Å) plans typical of anatase. The HR-TEM images presented in (B) and (D) correspond to the areas circled in (A) and in (C), respectively. The diffraction pattern presented in (E) correspond to the smaller area circled on graph (C).

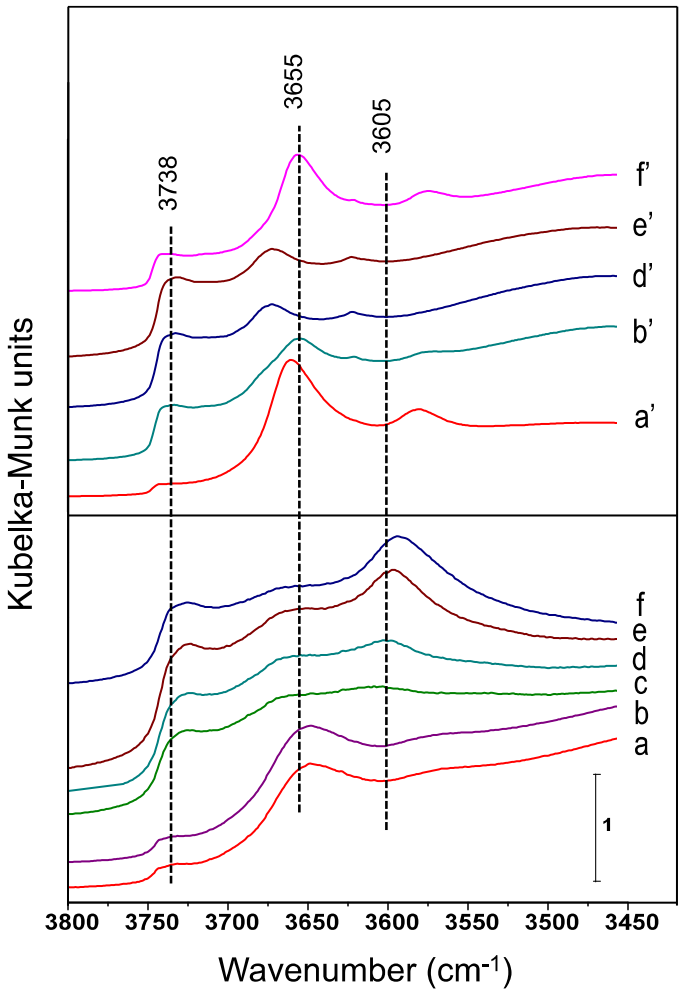

Figure 4 DRIFT spectra during calcination of the MOR samples contacted with the (a-f) $TiCl_3$ and (a'-f') $K_2TiO(C_2O_4)_2$ solutions, then washed and dried (50°C): spectra registered at (a,a') 25°C, (b) 100°C or (b') 150°C, (c) 200°C, (d,d') 300°C, (e,e') 450°C and (f,f') 25°C after cooling. The spectra are vertically shifted for the sake of better clarity.

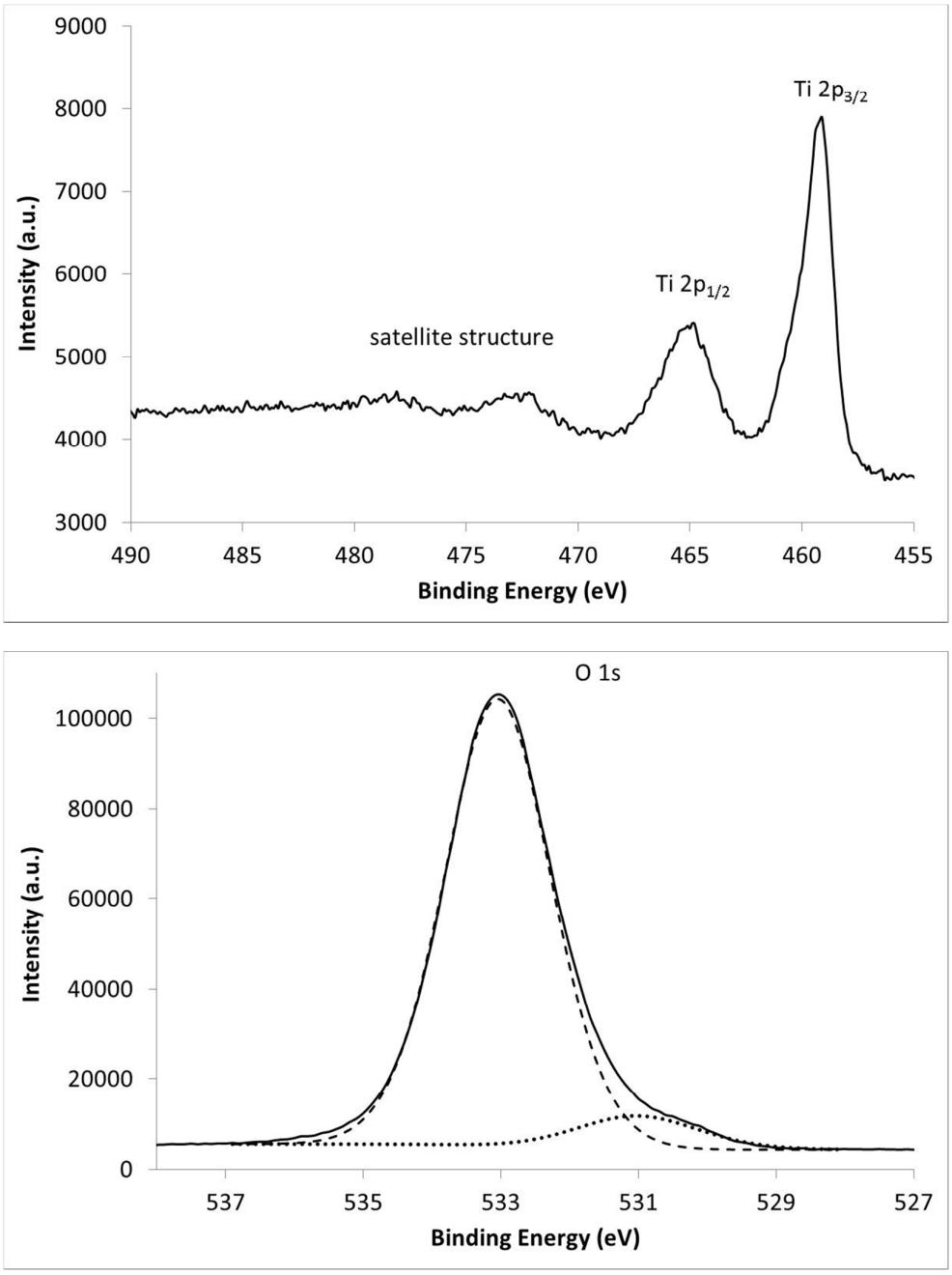

Figure 5: X-ray photoelectron spectra of TiO_2-$HMOR_{Cl}$ in the binding energies ranges characteristic of (a) Ti 2p and (b) O 1s.

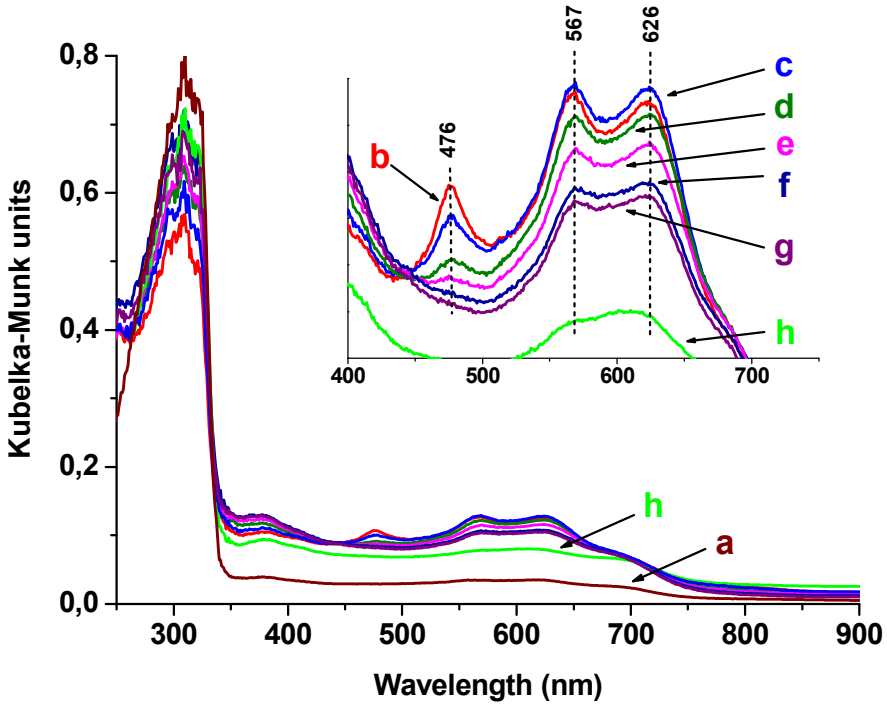

Figure 6: DRUVv spectra recorded as a function of time after laser irradiation at 300 nm of t-St@TiO_2-$HMOR_{Cl}$ (a) before irradiation, (b) 5 min, (c) 15 min, (d) 5 h, (e) 10 h, (f) 24 h, (g) 1.5 day and (h) 3 days after photoexcitation.

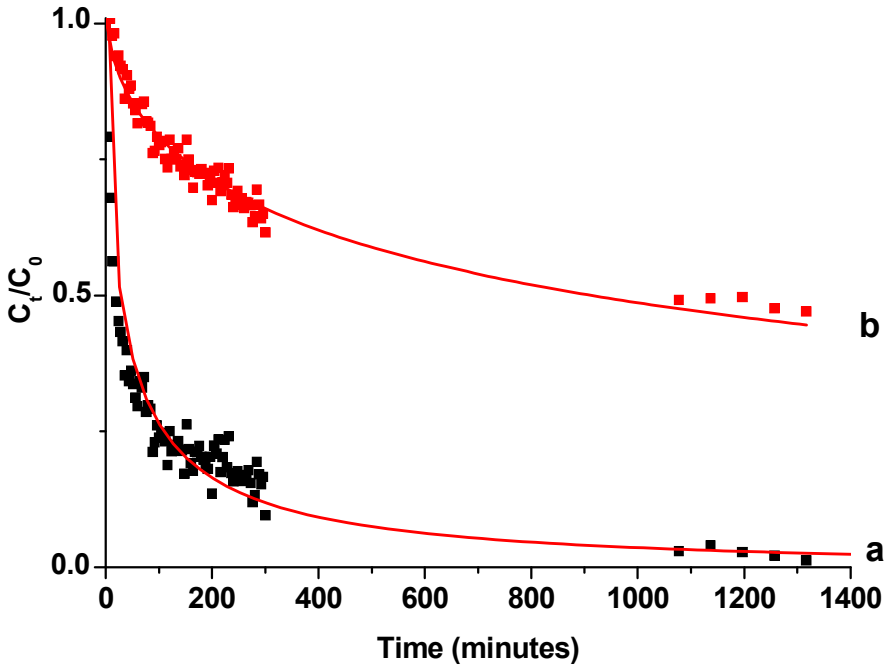

Figure 7. Normalized decay profiles of C_t/C_0 relative to spectral concentration of (a) t-$St^{\bullet+}$@TiO_2-H-$MOR_{Cl}^{\bullet-}$ and (b) t-St@TiO_2-$HMOR_{Cl}^{\bullet+\bullet-}$ monitored at 476 nm and at 567 nm respectively after the 300 nm laser excitation. The solid line represents the best fit calculated decays using the Albery function; the squares represent the experimental points.

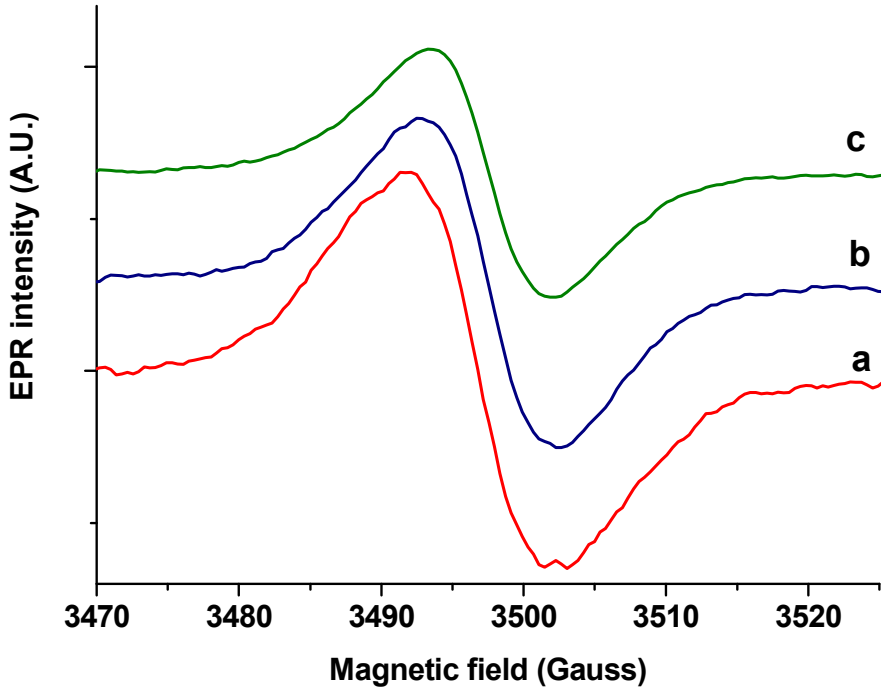

Figure 8. CW EPR spectra at room temperature after laser photoirradiation at 300 nm of t-St@TiO_2/$HMOR_{Cl}$; spectra recorded after (a) 10 min, (b) 2 h and (c) 1 day.

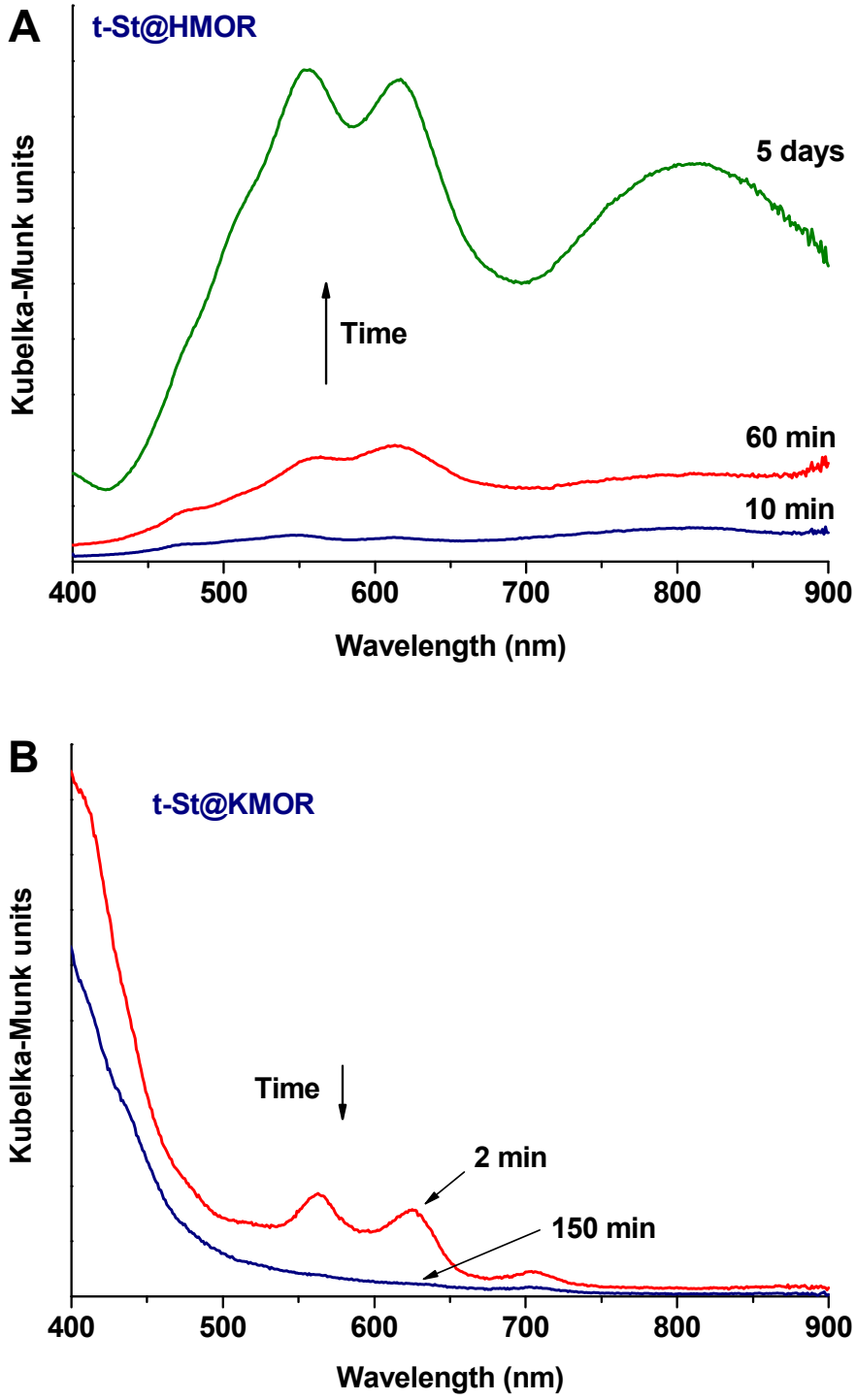

Figure S1: A) Evolution of the DRUVv spectra as a function of time after mixing t-St and acid H-MOR (spontaneous ionization). B) Evolution of the DRUVv spectra as a function of time after photoexcitation of t-St occluded in K-MOR (photoinduced ionization).

Graphical abstract

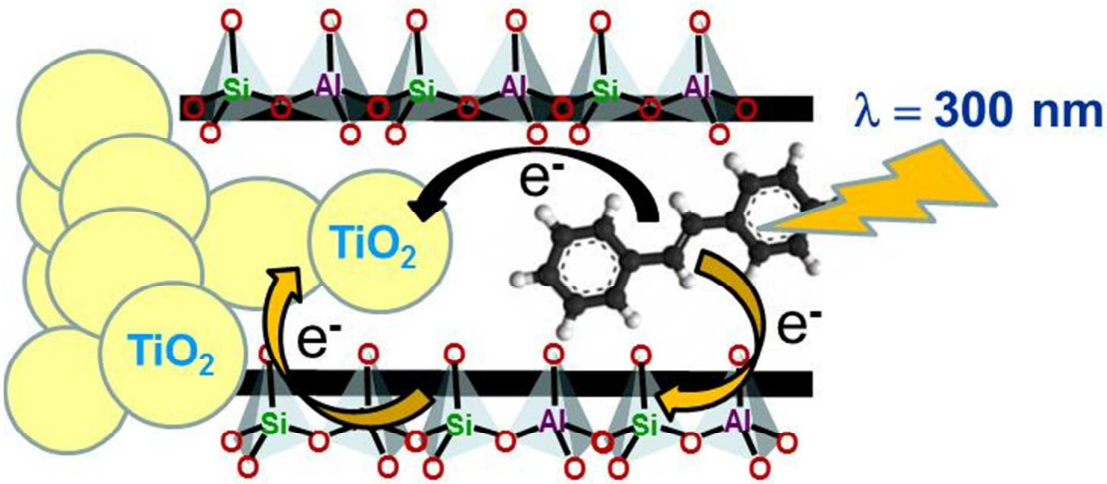

Ionization of a guest molecule occluded in TiO_2-containing zeolite and electron transfers towards the conduction band of the conductive material placed nearby.

Graphical abstract

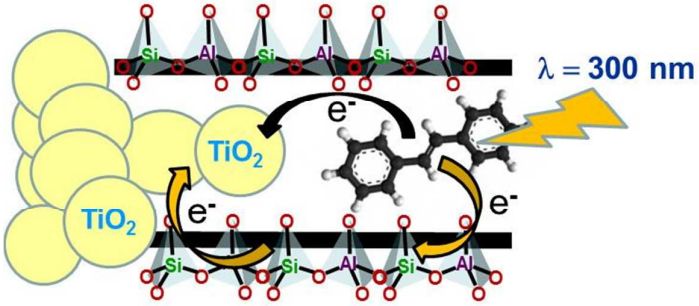

Ionization of a guest molecule occluded in TiO_2-containing zeolite and electron transfers towards the conduction band of the conductive material placed nearby.